Testing the Symmetric Assumption of Complementary Relationship: A Comparison between the Linear and Nonlinear Advection-Aridity Models in a Large Ephemeral Lake

Guojing Gan [1,2] , **Yuanbo Liu [1,]*** , **Xin Pan [3]** , **Xiaosong Zhao [1,2]** , **Mei Li [4] and Shigang Wang [5]**

1   Nanjing Institute of Geography and Limnology, Chinese Academy of Sciences, Nanjing 210008, China
2   Key Laboratory of Watershed Geographic Sciences, Chinese Academy of Sciences, Nanjing 210008, China
3   School of Earth Science and Engineering, Hohai University, Nanjing 211100, China
4   Hydrological Bureau of Jingdezhen City, Jingdezhen 333003, China
5   Hydrological Bureau of Poyang Lake, Jiujiang 332800, China
*   Correspondence: ybliu@niglas.ac.cn.com

Abstract: The accuracy of a complementary relationship (CR) evapotranspiration (ET) model depends on how to parameterize the relationship between apparent potential ET and actual ET as the land surface changes from wet to dry. Yet, the validity of its inherent symmetric assumption of the original CR framework, i.e., the B value equal to one, is controversial. In this study, we conduct a comparative study between a linear, symmetric version (B = 1) and a nonlinear, asymmetric version (B is not necessarily equal to 1) of the advection-aridity (AA) CR model in a large ephemeral lake, which experiences dramatic changes in surface/atmosphere humidity. The results show that B was typically 1.1 ± 1.4 when $ET \leq ET_{PT} \leq ET_{PM}$, where ET_{PM} and ET_{PT} are estimated using the Penman (PM) and Priestley–Taylor (PT) equations, respectively; the AA model performed reasonably well in this case. However, the value of B can be negative and deviate from 1 significantly if the inequality $ET \leq ET_{PT} \leq ET_{PM}$ is violated, which is quite common in humid environments. Because the actual ET can be negatively (B > 0) or positively (B < 0) related to the evaporative demand of the air, the nonlinear AA model generally performs better than the AA model if $ET \leq ET_{PM}$ is satisfied. Although B is not significantly correlated with the atmospheric relative humidity (RH), both models, especially the nonlinear AA model, resulted in negative biases when $ET > ET_{PM}$, which generally occur at high RH conditions. Both the linear and the nonlinear AA models performed better under higher water level conditions, however, our study highlights the need for higher-order (≥3) polynomial functions when CR models are applied in humid environments.

Keywords: complementary relationship; Advection-Aridity ET models; surface/atmosphere humidity changes

1. Introduction

Evapotranspiration (ET), which refers to water vapor transfer from the land surface to the atmosphere [1], serves as a key variable in hydrological and ecological cycles [2–4]. Numerous ET models [5–7] have been proposed in the past 50 years, among which complementary relationship (CR) models have been widely used because of their simple formulation and relatively few input requirements. The actual ET [8,9] or, specifically, its component, soil evaporation [10–12], can be readily estimated using the CR concept and meteorological variables. Additionally, CR provides a simple but useful tool for evaluating global hydrological responses to climate change [13,14].

CR was first proposed by Bouchet [15] and was further developed by many others [16–23]. CR refers to the opposite behaviors of the actual ET (ET_a) and the apparent potential ET (ET_{pa}) when they deviate from the potential evaporation (ET_{po}) as the land surface changes from completely wet to completely dry. ET_a of a large uniform area occurs at its potential rate (ET_{po}) if the evaporating surface is saturated and the ambient air is fully adjusted to the saturation condition of the surface. ET_{pa}, which is usually represented by pan evaporation, also equals ET_{po} in this case. Therefore, as the land surface becomes dry, ET_a decreases due to the limited water supply, whereas ET_{pa} increases because of the extra sensible energy, i.e., $Q_1 = ET_{po} - ET_a$, will be used to increase ET_{pa} by the amount of Q_2, where $Q_2 = ET_{pa} - ET_{po}$. $B = Q_2/Q_1$ represents the ratio of the sensible energy that has been used in increasing the evaporative demand of the air. B has to be parameterized in CR applications. For example, the aridity-advection (AA) model [16] assumes that B = 1, i.e., $ET_{pa} - ET_{po} = ET_{po} - ET_a$. Therefore, actual ET can be estimated readily from the potential and apparent potential ET, $ET_a = 2$ $ET_{po} - ET_{pa}$. Although the AA model has been intensively used at various spatial and temporal scales, e.g., catchment scales [24], local-site scales [25], daily scales [26] and sub-daily scales [27], studies have shown that Q_2 is not necessarily equal to Q_1 under local advection conditions [26,28]. Szilagyi [29] concluded that the symmetric assumption is valid only when no energy exchange occurs between the source of ET_{pa} and its surroundings. Recently, Brutsaert [21] formulated a nonlinear version of the AA model (denoted as NAA in this paper) by invoking a generalized complementary principle with physical constraints, thus eliminating the B = 1 assumption. The NAA model has been tested using flux measurements or water balance results under various climatic and vegetation conditions [30–33]. However, few studies have compared the applicability of the linear (B = 1) and nonlinear (B is not necessarily equal to 1) AA models.

Note that CR describes the ET of the land surface that changes from completely wet to completely dry. However, few studies have examined the utility of the CR models and the B = 1 assumption under an environment that experiences large humidity variations in both the land surface and the atmosphere. In addition, by definition, $ET \leq ET_{po} \leq ET_{pa}$ is valid in any circumstances. However, ET_{pa} and ET_{po} are usually estimated using the Penman (PM) and Priestley–Taylor (PT) equations, respectively. At humid conditions, the equality $ET \leq ET_{PT} \leq ET_{PM}$ can be violated, which may introduce errors in CR applications. In this paper, we conduct a comparative study between the AA and NAA models in a large ephemeral lake and examine the variations in B under different saturation conditions. The eddy covariance (EC) system that was located in an ephemeral lake provides ET measurements under the land surface and water surface conditions.

2. Model Description and General Definitions

Potential evaporation (ET_{po}, W/m^2) refers to the evaporation rate of a large uniform saturated surface where the ambient air has been fully adjusted to the saturation condition of the surface. ET_{po} is mainly controlled by the available energy, i.e., $R_n - G$, where R_n and G are the net radiation (W/m^2) and soil heat flux (W/m^2), respectively. ET_{po} is usually estimated using the Priestley–Taylor equation [34], ET_{PT}, as shown in Equation (1), where Δ (hPa/K) is the slope of the saturated vapor pressure to the air temperature and γ (hPa/K) is the psychrometric constant. Δ and γ are functions of air temperature and air pressure, respectively. α is a parameter that is widely accepted as 1.26 from the work of Priestley and Taylor [34].

$$ET_{po} = \alpha \frac{\Delta}{\Delta + \gamma}(R_n - G) \tag{1}$$

Apparent potential evaporation ET_{pa} (W/m^2) refers to the evaporation rate of a small saturated surface, e.g., the evaporating pan, which is surrounded by a large non-saturated homogeneous surface. ET_{pa} thus represents the evaporative demand of the air. ET_{pa} can be represented using pan evaporation measurements or can be estimated using the Penman equation [35], ET_{PM}, as shown in Equation (2). E_a is calculated as the product of the vapor pressure deficit (VPD, hPa) and the wind function, i.e.,

$f(u_2) = 7.43 \times (1 + 0.54u_2)$ [36], where u_2 is the wind speed at the height of 2 m. u_2 is estimated using the wind speed measurement u_r at the height of z_r [37].

$$ET_{PM} = \frac{\Delta}{\Delta + \gamma}(R_n - G) + \frac{\gamma}{\Delta + \gamma}E_a \tag{2}$$

$$u_2 = u_r(2/z_r)^{1/7} \tag{3}$$

Both ET_a and ET_{pa} are equal to ET_{po} when the surface and the atmosphere are both saturated. As the evaporating surface changes from wet to dry, ET_{pa} increases, whereas ET_a decreases. The original AA model [16] states that the deviations of ET_{pa} and ET_a with ET_{po} are equal to each other, i.e., $ET_{pa} - ET_{po} = ET_{po} - ET_a$. Therefore, the actual ET can be estimated using ET_{po} and ET_{pa}, as shown as follows:

$$ET_a = 2ET_{po} - ET_{pa} \tag{4}$$

Brutsaert [21] abandoned the assumption that $ET_{pa} - ET_{po} = ET_{po} - ET_a$. Instead, he solved a more generalized function $y = x - \sum a_i x^i$ (i = 0, … , n), where $x = ET_{po}/ET_{pa}$, and $y = ET_a/ET_{pa}$, by invoking the physical constraints as boundary conditions, as shown as follows.

$$\begin{aligned} y &= 1, \quad x = 1 \\ y &= 0, \quad x = 0 \\ \frac{dy}{dx} &= 1, \quad x = 1 \\ \frac{dy}{dx} &= 0, \quad x = 0 \end{aligned} \tag{5}$$

A cubic polynomial equation satisfies the four boundary conditions, i.e.,

$$y = 2x^2 - x^3 \tag{6}$$

or, in terms of ET,

$$ET_a = \left(\frac{ET_{po}}{ET_{pa}}\right)^2 (2ET_{pa} - ET_{po}) \tag{7}$$

When applying the AA and the NAA model, ET_{pa} and ET_{po} are substituted by ET_{PM} and ET_{PT}. ET_{PM} and ET_{PT} are mainly used in the subsequent analysis in the rest of the paper.

3. Study Area and Data Processing

We use EC and meteorological measurements from Poyang Lake (28°22′–29°45′ N, 115°47′–116°45′ E) in this study. Poyang Lake is located on the south bank of the Yangtze River (Figure 1). The Poyang Lake basin is characterized as humid subtropical climate. Annual mean air temperature is 17.5 °C and mean annual precipitation is 1635.9 mm for 1960–2010. Precipitation is the largest in April, May, and June, and decreases sharply from July to September [38]. Five rivers (Xiushui, Ganjiang, Fuhe, Xinjiang, and Raohe) are the main water suppliers to the lake [39], and the lake discharges to the Yangtze River at Hukou (Figure 1). The inundated area of Poyang Lake varies remarkably from more than 3000 km^2 in summer to less than 1000 km^2 in winter [39–41].

Eddy covariance and meteorological devices were mounted on a 38-m tower (29.09° N, 116.38° E) on Sheshan Island (Figure 1), which is located in a periodically inundated zone of Poyang Lake. Xingzi station is the most representative site of the overall water level status of Poyang Lake [42]. The water surface coverage within the EC footprint ranges from >90% when the water level at Xingzi station is greater than 14 m to less than 20% when the water level is less than 12 m during the low-water period [43]. The EC system thus measures the latent heat flux (LE, equivalence to ET in energy units, W/m^2) from the water surface and land surface during the high-water and low-water periods, respectively. In addition, surface radiation components, including the downward/upward short-wave and long-wave radiation are measured by the pyrgeometers/pyranometers (CNR4, Kipp & Zonen B.V.,

Delft, The Netherlands), and the air temperature and relative humidity are measured by HMP155A (Vaisala, Helsinki, Finland).
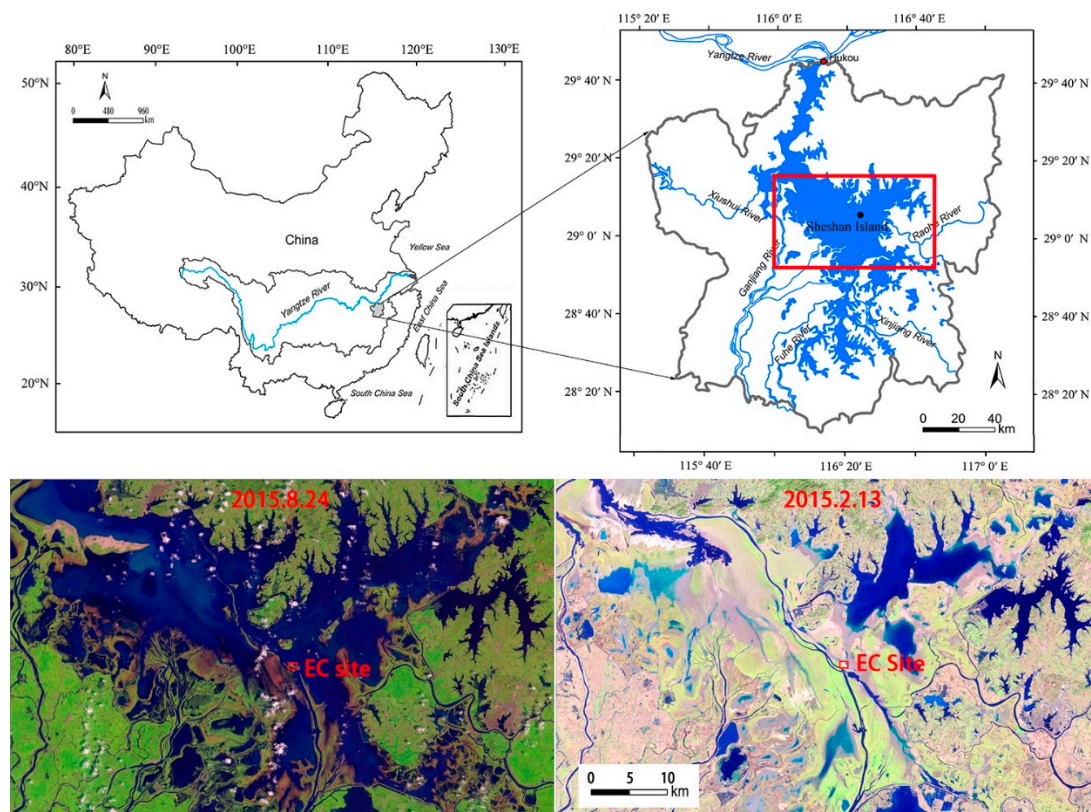
Figure 1. The study area and the measuring site in Sheshan Island. Surroundings of the measuring site are revealed using Landsat 8 images acquired at 24 August (high-water) and 13 February (low-water), 2015.

Nighttime data were not used to avoid the underestimation of LE under low turbulence conditions. Moreover, the data points at which the available energy (H + LE) is smaller than 10 W/m^2 were also discarded. Therefore, the data at the timings when the downward shortwave radiation and the available energy were larger than 10 W/m^2 within a day were aggregated to the daily scales for analysis. Daily data (1 January–21 December 2015) from Poyang Lake were used for the analysis in this study.

4. Results

4.1. Seasonal Variations in Surface/Atmosphere Humidity Conditions

The water level (WL) of Poyang Lake usually experiences dramatic seasonal changes. In 2015, the WL fluctuated from 7.6 to 19.5 m, with the minimum and maximum values occurring on DOY 48 and DOY 175, respectively (Figure 2A). The WL was approximately 8 m in January and February when the bottom of the lake region was exposed with mudflat and short grass. The WL rose to an average of 11.9 m during March and April, and then rose rapidly to an average of 16.0 m during May and June. Mixed footprints (water + land) existed during March and April, whereas footprints basically consisted of the water surface in May and June. The EC system still measured the water surface evaporation during July and August, when the WL was 16.1 m on average. The WL fell to an average of 13.1 m during September and October, and an average of 12.7 m during November and December. The lake bottom was exposed for only a short period around DOY 310 when the WL was less than 12 m.
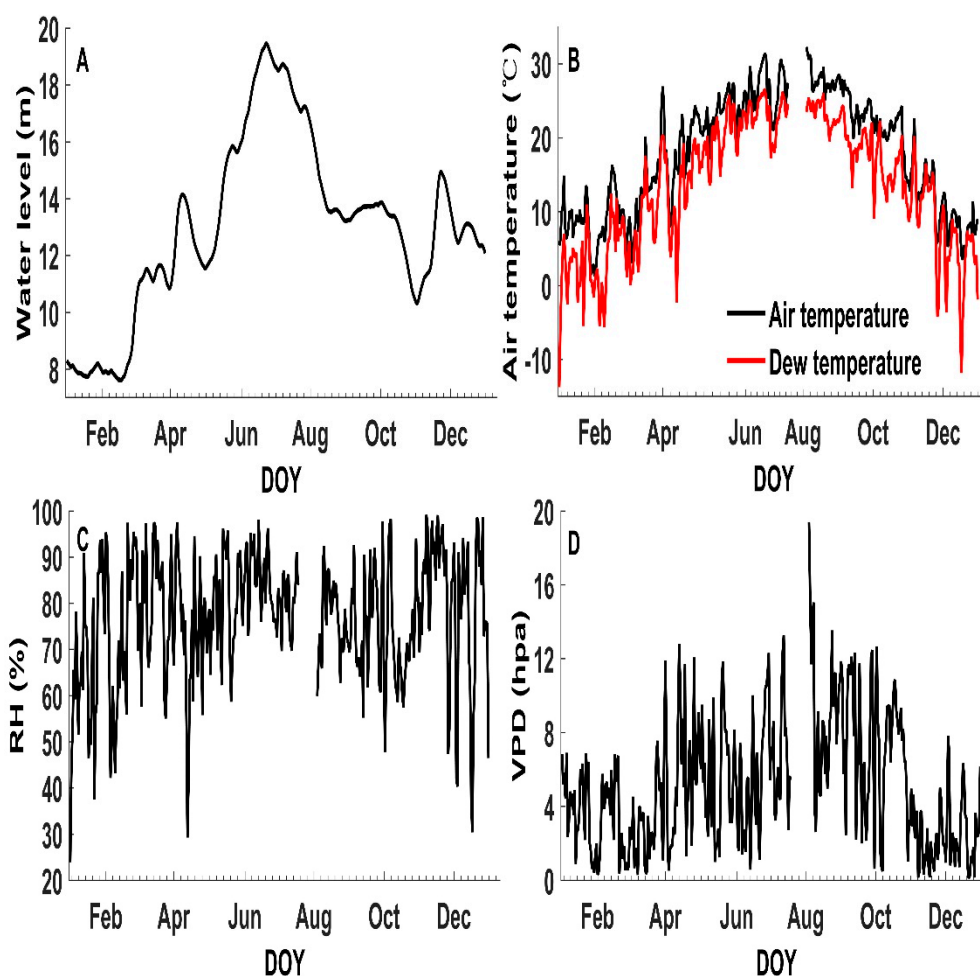
Figure 2. Seasonal variations in the (**A**) water level (Xingzi station), (**B**) air temperature, dew temperature, (**C**) relative humidity and (**D**) VPD in 2015. DOY is day of the year.

A single-peak sinusoidal seasonal cycle was found for the air temperature (T_a) (Figure 2B). The minimum T_a was still larger than 0 °C, whereas the maximum reached approximately 30 °C. The dew temperature (T_d) was an average of 4.4 °C lower than T_a. The difference between T_a and T_d was highly correlated (-0.99) with relative humidity (RH). RH was generally higher during the period of high WL. However, RH also reached as high as 80% when WL was the lowest, e.g., from January to March. In contrast, VPD during January to March was generally smaller than in the high-water period because the saturated vapor pressure of the air was lower in the spring due to the low T_a.

4.2. CR under Different Surface/Atmosphere Humidity Conditions

The relationships between LE and the apparent potential LE are shown in Figure 3 under different surface/atmosphere humidity conditions. For proper demonstration, the y-axis was scaled using LE_{PT}. Superficially, the scatter points in Figure 3 do not seem to conform to one single pattern. However, we observe that in the high RH ($\geq$85%) and $LE/LE_{PM} > 1$ condition, LE/LE_{PT} increases as LE/LE_{PM} increases. In addition, when the ideal inequality $LE \leq LE_{PT} \leq LE_{PM}$ is met, LE_{PM}/LE_{PT} and LE/LE_{PT} exhibit opposite trends as LE/LE_{PM} increases, as shown in the fitted line in Figure 3. The rest of the data points, e.g., those in the ellipse in Figure 3A, occur when both LE_{PM}/LE_{PT} and LE/LE_{PT} are larger than 1.

Therefore, for proper demonstration, we divided the dataset into three categories. Category 1 satisfies the ideal inequality $LE \leq LE_{PT} \leq LE_{PM}$. Category 2 violates the inequality $LE \leq LE_{PT} \leq LE_{PM}$ but still satisfies the inequality $LE \leq LE_{PM}$, i.e., LE may be larger than LE_{PT} or LE_{PT} may be larger than

LE_{PM} in this category (e.g., those in the ellipse in Figure 3A). Category 3 contains the data points where LE is larger than LE_{PM}, which generally occurs under RH ≥ 85% conditions. Notably, each category broadly exists in all water level conditions (Figure 3). The number of data points in each category is shown in Table 1. Category 1 and 3 consist of 27.4% and 28.1% of the total data, respectively, and category 2 accounts for the largest proportion of the data. The proportion of data in category 1 reaches its maximum in the period of January and February when the lake bottom is rarely covered by water. As the water level rises, the proportion of data in category 1 in the entire dataset generally decreases, especially during the rapid water-rising period, e.g., May and June.
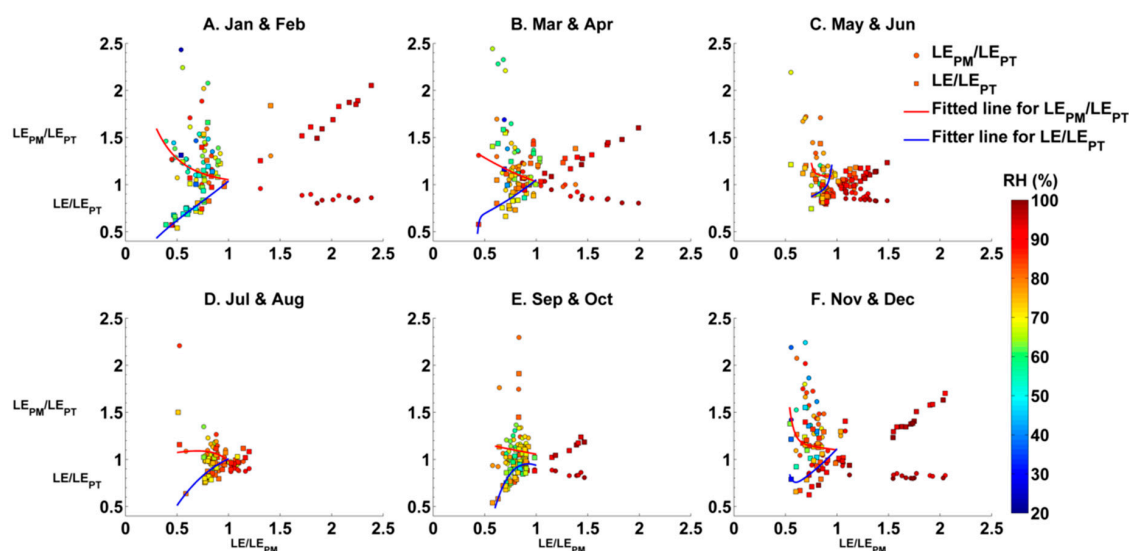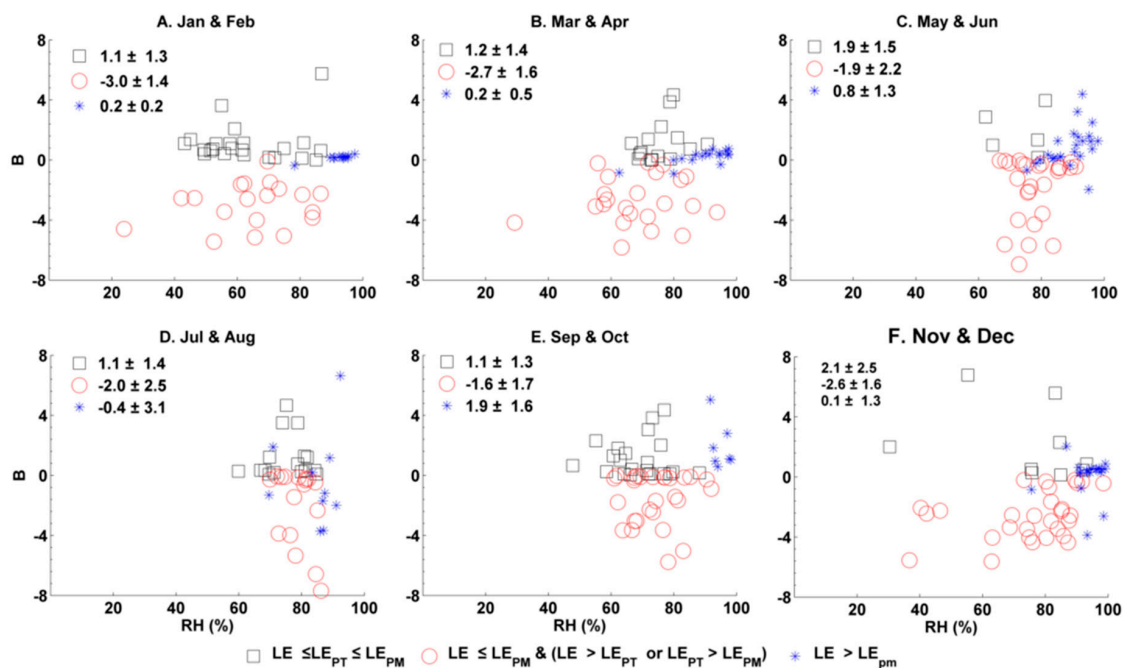

Figure 3. Complementary relationship under various water level and atmospheric humidity conditions throughout the year. (**A**), Jan and Feb; (**B**), Mar and Apr; (**C**), May and Jun; (**D**), Jul and Aug; (**E**), Sep and Oct; (**F**), Nov and Dec.

Table 1. Numbers of data points in each category.

Date	Category 1 $LE \leq LE_{PT} \leq LE_{PM}$	Category 2 $LE \leq LE_{PM}$ AND ($LE \geq LE_{PT}$ OR $LE_{PT} \geq LE_{PM}$)	Category 3 $LE \geq LE_{PM}$	Total
January & February	23	19	12	54
March & April	15	23	17	55
May & June	5	26	24	55
July & August	16	17	10	43
September & October	22	27	7	56
November & December	9	29	19	57

When $LE \leq LE_{PT} \leq LE_{PM}$, LE_{PM}/LE_{PT} and LE/LE_{PT} exhibit opposite trends as LE/LE_{PM} increases (Figure 3). Both the upper (LE_{PM}/LE_{PT}) and lower (LE/LE_{PT}) scatter points in Figure 3 were fitted using exponential functions. The slopes of the fitted LE_{PM}/LE_{PT} curves are generally smaller in high-water periods, whereas the slopes of the lower line exhibit no significant changes with the water level. Both LE_{PM}/LE_{PT} and LE/LE_{PT} do not seem to be significantly correlated with RH (Figure 3). In addition, the B values exhibit no significant trends with RH or the water level. The mean values of B are approximately 1.1 during most of the periods (Figure 4A,B,D,E), indicating that the AA model assumption is generally feasible for category 1 data. However, the value of B can also be close to 2 during the rapid water-rising periods, e.g., May and June, and November and December. It is worth noting that the number of data points during the rapid water-rising periods is much smaller than in other periods.

Figure 4. The relationship between B and RH under various water level conditions throughout the year. (**A**), Jan and Feb; (**B**), Mar and Apr; (**C**), May and Jun; (**D**), Jul and Aug; (**E**), Sep and Oct; (**F**), Nov and Dec.

The value of B is generally negative for category 2 data because LE_{PT} is usually smaller than both LE and LE_{PM} (Figure 3). The negative value of B in the equation $LE_{PM} - LE_{PT} = B (LE_{PT} - LE)$ implies that LE increases rather than decreases with increasing atmospheric demand (LE_{PM}). Note that the B values in this category do not seem to exhibit significant trends with RH. However, the distribution of B is correlated with the water level. B is much closer to 0 during the high-water periods, i.e., May to October. The mean values of B are −1.9, −2.0 and −1.6 in Figure 4C–E, respectively, which are larger than those in other periods (Figure 4A,B,F). In addition, more data points are distributed approximately 0 from May to October than in other periods. One main reason for this phenomenon may be because LE_{PT} is close to LE_{PM} for water-covered surfaces.

The $LE \geq LE_{PM}$ cases (category 3) generally occur when RH is relatively large (>85%). Note that most of the points in category 3 satisfy the inequality $LE \geq LE_{PT} \geq LE_{PM}$; therefore, B is generally positive in category 3. Compared to category 2, the value of B in category 3 is much closer to 0 during the low-water periods, which is shown in Figure 4A,B,F.

### 4.3. Comparison of the AA and the NAA Simulations on the $LE_{PT}/LE_{PM} \sim LE/LE_{PM}$ Relationship

Let $x = LE_{PT}/LE_{PM}$ and $y = LE/LE_{PM}$; then, we can rewrite $LE_{PM} - LE_{PT} = B (LE_{PT} - LE_a)$ as $y = \frac{B+1}{B}x - \frac{1}{B}$. As shown in Section 2, the AA model assumes that B equals 1, i.e., $y = 2x - 1$. In contrast, the NAA model obtained a nonlinear formulation from a more general perspective (B is not a fixed value), i.e., $y = 2x^2 - x^3$. The performances of the AA and the NAA models in simulating the $LE_{PT}/LE_{PM} \sim LE/LE_{PM}$ relationships are shown in Figure 5.

The results showed that the nonlinear formulation generally performed better than the AA model. For example, the Root mean square error (RMSE) of the AA and NAA models were 0.24 and 0.15, respectively, during May and June. The RMSE of the two models were close to each other during January and February; however, the absolute bias of the NAA model was smaller than that of the AA model. Moreover, the model performances were found to be related to humidity conditions. For example, both the AA and the NAA models performed better during the periods with the highest water level (Figure 5C,D) than during the low-water periods. Large negative (<−0.10) biases were

found during the low-water periods (Figure 5A,B,F) for both the AA and the NAA models. One main reason for such large negative biases is the underestimation of the models when the air is near saturated, i.e., RH > 85% (Figure 5A,B,F).
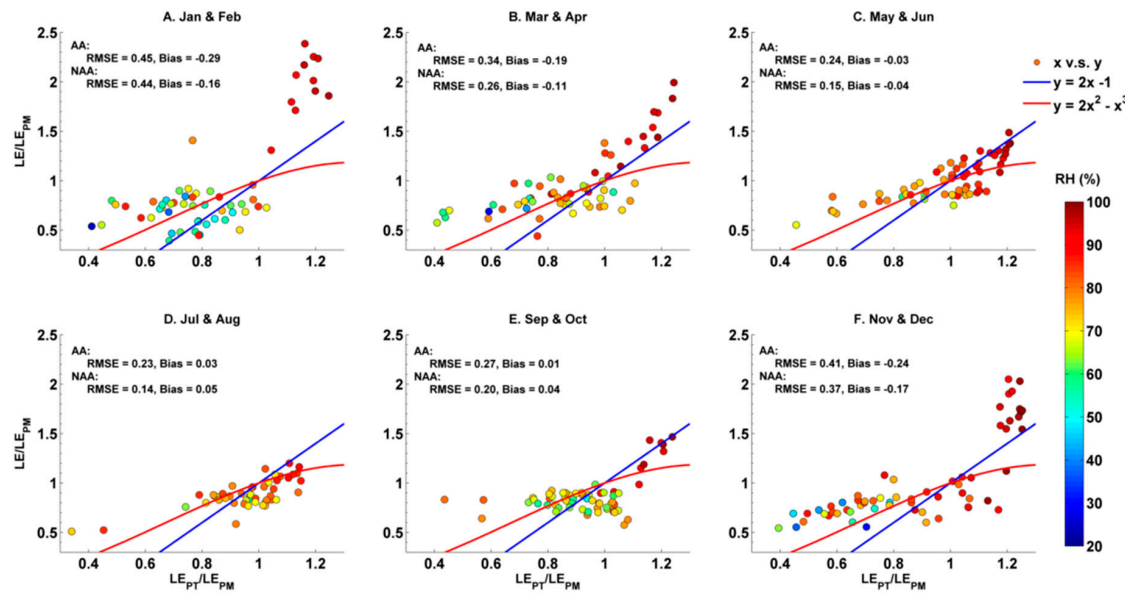
Figure 5. Performances of the advection-aridity (AA) and nonlinear version of the AA model (NAA) models in simulating the relationships between LE_{PT}/LE_{PM} and LE/LE_{PM}. (**A**), Jan and Feb; (**B**), Mar and Apr; (**C**), May and Jun; (**D**), Jul and Aug; (**E**), Sep and Oct; (**F**), Nov and Dec.
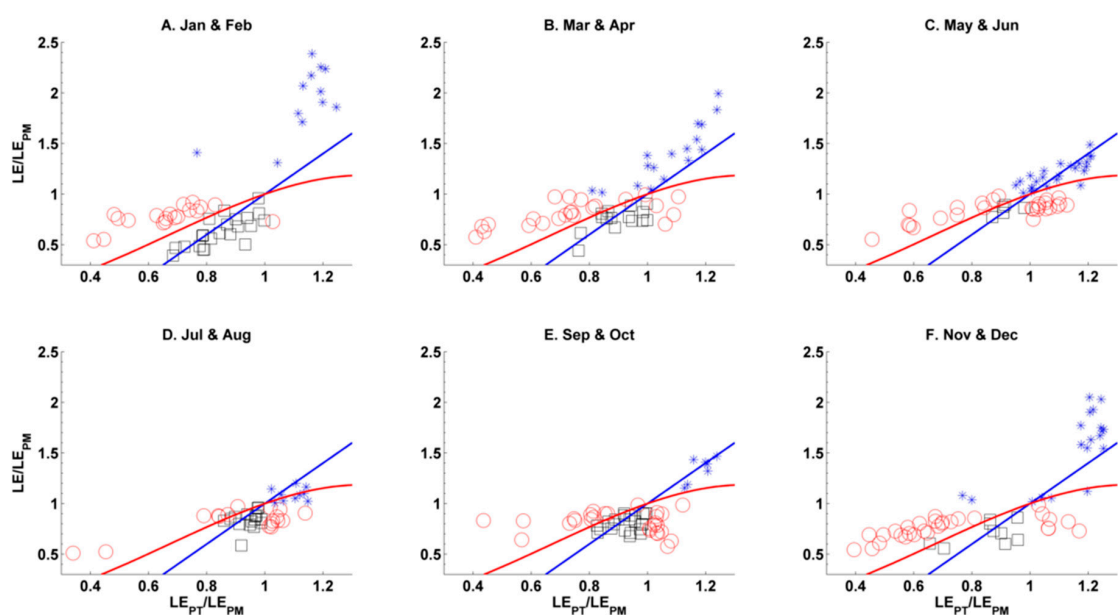
Figure 6. Performances of the AA and NAA models in simulating the relationships between x and y in three data categories, where x = LE_{PT}/LE_{PM}, and y = LE/LE_{PM}. (**A**), Jan and Feb; (**B**), Mar and Apr; (**C**), May and Jun; (**D**), Jul and Aug; (**E**), Sep and Oct; (**F**), Nov and Dec.

More detailed examinations show that the linear formulation y = 2x − 1 performed reasonably well for the data points that satisfied the inequality $LE \leq LE_{PT} \leq LE_{PM}$ (category 1) (Figure 6). However, for category 2, y = 2x − 1 underestimates LE/LE_{PM} at most of the points, especially when LE_{PT}/LE_{PM} was smaller than 1. In contrast, the nonlinear x-y formulation (y = $2x^2 - x^3$) performed better than

the linear formulation for the data in category 2. However, the nonlinear formulation performed worse than the linear formulation for the data points in category 3. The nonlinear formulation greatly underestimated LE/LE$_{PM}$ at high humidity conditions because $y = 2x^2 - x^3$ increases much more slowly at high humidity conditions.

4.4. AA and NAA Model Performances in Estimating LE

Performances of the AA and the NAA models in estimating LE are analyzed in this section. Overall, the AA model had a 35.6 W/m^2 RMSE and a −8.8 W/m^2 mean bias, whereas the NAA model had comparable accuracy, i.e., a 36.9 W/m^2 RMSE and a −6.4 W/m^2 mean bias. Both the AA and the NAA models produced similar trends compared to the measured LE time series (Figure 7). However, the AA model performed worse with larger negative biases than the NAA model when LE was relatively small (<150 W/m^2), as shown in Figure 7. In contrast, the NAA model resulted in larger negative biases than the AA model when the LE was larger than 200 W/m^2 (Figure 7).
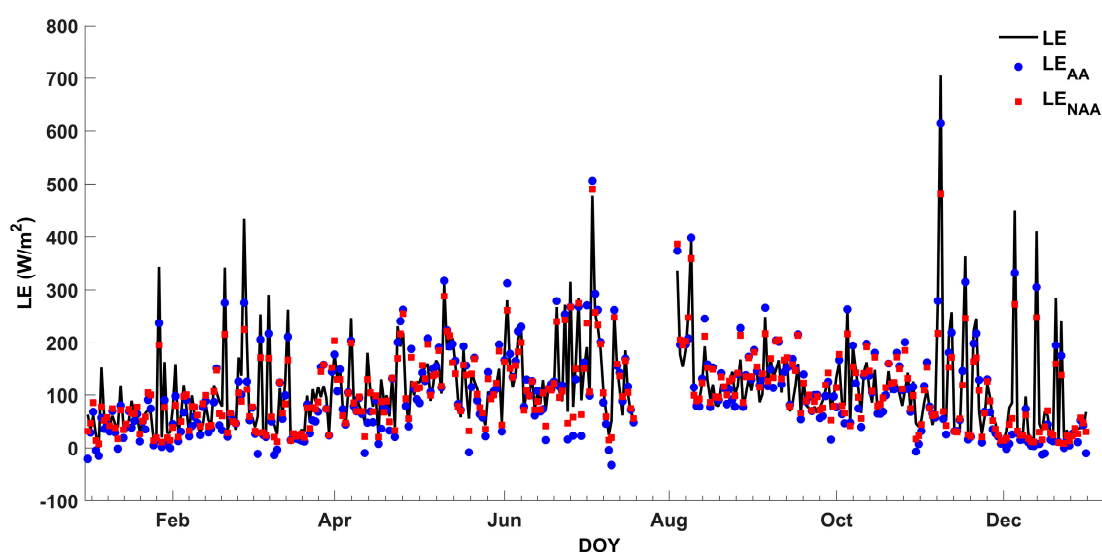

Figure 7. Comparisons between the time series of the measured latent heat flux (LE) and the modeled LE using the AA and NAA models.

The distribution of measured LE under various water level conditions is shown in Figure 8. LE was generally higher in the high-water periods. In addition, LE generally increased with LE$_{PT}$/LE$_{PM}$ (Figure 8). Worth noting, LE in category 1 was not significantly different from that in category 2, whereas most of the highest LE values are for data in category 3. The AA model performed reasonably well in simulating LE in category 1 (Figure 9). Prediction biases were confined within ±50 W/m^2 and their averages were close to 0 for different water-level conditions. Prediction biases showed no significant trend with respect to atmospheric humidity (RH). Such a result indicates that the AA model is robust in estimating LE across different surface/atmospheric humidity conditions, if the inequality LE ≤ LE$_{PT}$ ≤ LE$_{PM}$ is met. In contrast, the prediction biases (absolute values) in category 2 decreased as RH increased in relatively low-water level periods (Figure 9A,B,F). The model simulations in category 2 were better during the relatively high-water periods (Figure 10C,D,E). Overall, model performances improved under humid surface/atmospheric conditions for the data points in category 2. In contrast, large negative biases resulted from the AA model simulation in category 3. However, for category 3, the model performances were also better during the high-water periods (Figure 10C,D,E) than during the relatively low-water period (Figure 10A,B,F). Compared to the AA modeling biases, the NAA model biases exhibited similar distributions under different water level and atmospheric humidity conditions (Figure 10). However, the NAA model outperformed the AA model for the data points in category 2 and performed worse for the category 3 data.
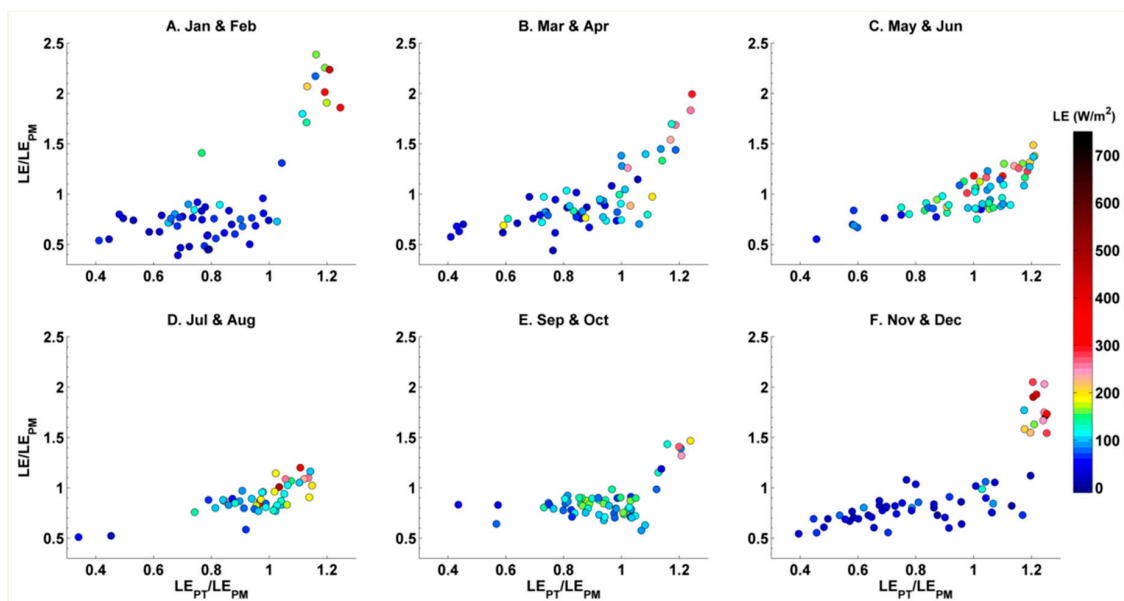
Figure 8. Distribution of LE with respect to the x-y plane under various water level conditions, where x = LE$_{PT}$/LE$_{PM}$, and y = LE/LE$_{PM}$. (**A**), Jan and Feb; (**B**), Mar and Apr; (**C**), May and Jun; (**D**), Jul and Aug; (**E**), Sep and Oct; (**F**), Nov and Dec.
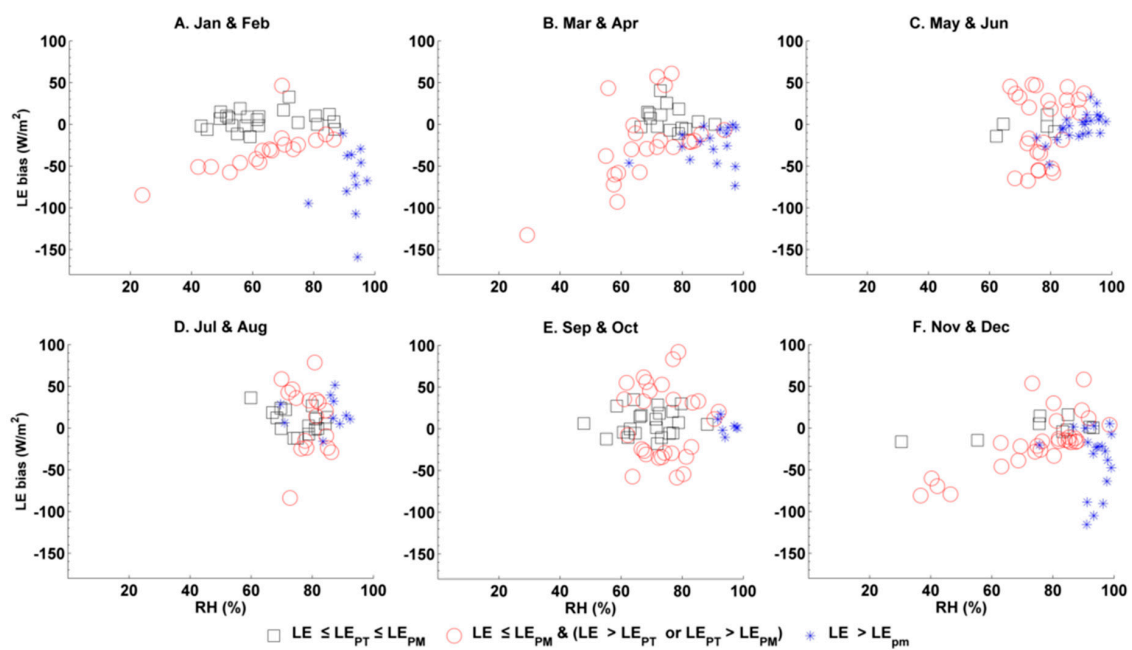
Figure 9. LE biases from the AA model under various water level and atmospheric humidity conditions. (**A**), Jan and Feb; (**B**), Mar and Apr; (**C**), May and Jun; (**D**), Jul and Aug; (**E**), Sep and Oct; (**F**), Nov and Dec.
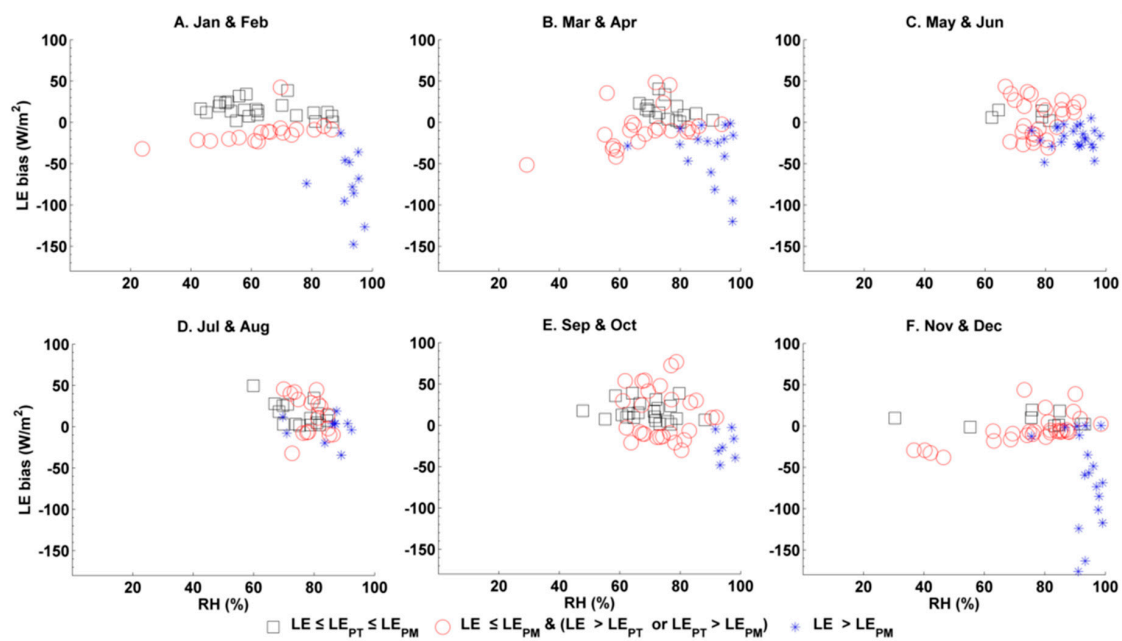
Figure 10. LE biases from the NAA model under various water level and atmospheric humidity conditions. (**A**), Jan and Feb; (**B**), Mar and Apr; (**C**), May and Jun; (**D**), Jul and Aug; (**E**), Sep and Oct; (**F**), Nov and Dec.

5. Discussion

By definition, the actual ET should be smaller than both the potential and the apparent potential ET, and the apparent potential ET should be the upper-most ET rate because it represents the evaporative demand of the air. Note that if LE_{po} and LE_{pa} are estimated using the PT and the PM equations, respectively, the inequality $LE \leq LE_{PT}$ is generally met in arid environments because of the limited water supply. The inequality $LE_{PT} \leq LE_{PM}$ is also easily met because the atmospheric evaporative demand is usually quite large (due to the hot dry/air in arid environments) compared to the available energy of the land surface in arid environments. Therefore, $LE \leq LE_{PT} \leq LE_{PM}$ is usually met in arid environments. However, in a humid climate environment such as in our study area, because the water supply for evaporation is usually adequate, LE/LE_{PT} may increase to be larger than 1 as LE_{PM}/LE_{PT} increases with the atmospheric evaporative demand. Examples of such cases can be found in the eclipse area in Figure 3A, where $LE/LE_{PT} > 1$. In addition, in high RH conditions (RH ≥ 85%), the LE_{PM} that is estimated using the Penman equation can be relatively small due to the relatively small VPD; thus LE/LE_{PM} can be larger than 1 as LE/LE_{PT} increases.

One way to avoid the violation of the inequality $LE \leq LE_{PT} \leq LE_{PM}$ is to adjust the parameter α in the LE_{PT} estimation. Numerous studies have shown that α can vary around its recommended value (1.26) for land surfaces [44–47]. Furthermore, α varies even under water body conditions [48,49]. However, no consistent parameterization of α has been established. A prior α is often used in CR applications. Therefore, violations of the inequality $LE \leq LE_{PT} \leq LE_{PM}$ are usually inevitable.

Our results indicated that the relationships between x and y differ significantly depending on the magnitude order in LE, LE_{PT} and LE_{PM}. For example, for $LE \leq LE_{PT} \leq LE_{PM}$ cases (category 1), the average values of parameter B vary around 1.1~2.1 with different WL conditions (Figure 4A–F). A linear equation $y = 1.625x − 0.63$ results if B is taken as the median value, 1.6, indicating that the AA model ($y = 2x − 1$) is quite accurate for the data points that satisfy the inequality $LE \leq LE_{PT} \leq LE_{PM}$. The AA model predicts that LE will be 0 when LE_{PT} equals half of LE_{PM}, i.e., $y = 0$ when $x = 0.5$. The tendency of the data points in category 1 seems to satisfy this character. However, our data show that in category 2, y is still positive when x is smaller than 0.5 (Figure 6). The intercepts of the linear regressions of the data in category 2 seem to be positive instead of negative as in the AA

model. The average values of the parameter B vary around $-3.0 \sim -1.9$ for category 2. A linear equation $y = 0.6x + 0.4$ results if B is taken as -2.5. Therefore, in terms of ET, $ET_a = 0.6ET_{PT} + 0.4ET_{PM}$. Such a result indicates that the actual ET increases instead of decreasing with increasing ET_{pa}. Note that the increase in the actual ET with ET_{PM} is not contradictory to the CR [50], and there are also many studies that have reported that y is still positive when x is smaller than 0.5, even in arid and semi-arid environments [20,31]. Nevertheless, the slope and intercept of the linear equation $y = 0.6x + 0.4$ is significantly different from that in the AA model.

From a modeling perspective, LE is not known a priori; therefore, the magnitude order in LE, LE_{PT} and LE_{PM} is not known. Whether a data point belongs to category 1 or category 2 cannot easily be determined in advance for humid environments. Higher-order polynomial equations such as the nonlinear AA model may be more useful than linear equations. We further fitted the x-y relationships using quadratic polynomial equations (Figure 11). The mean biases are close to 0, which are much smaller than those from the AA and the NAA models. RMSE values from the quadratic functions are approximately half of the values from the AA and the NAA models.
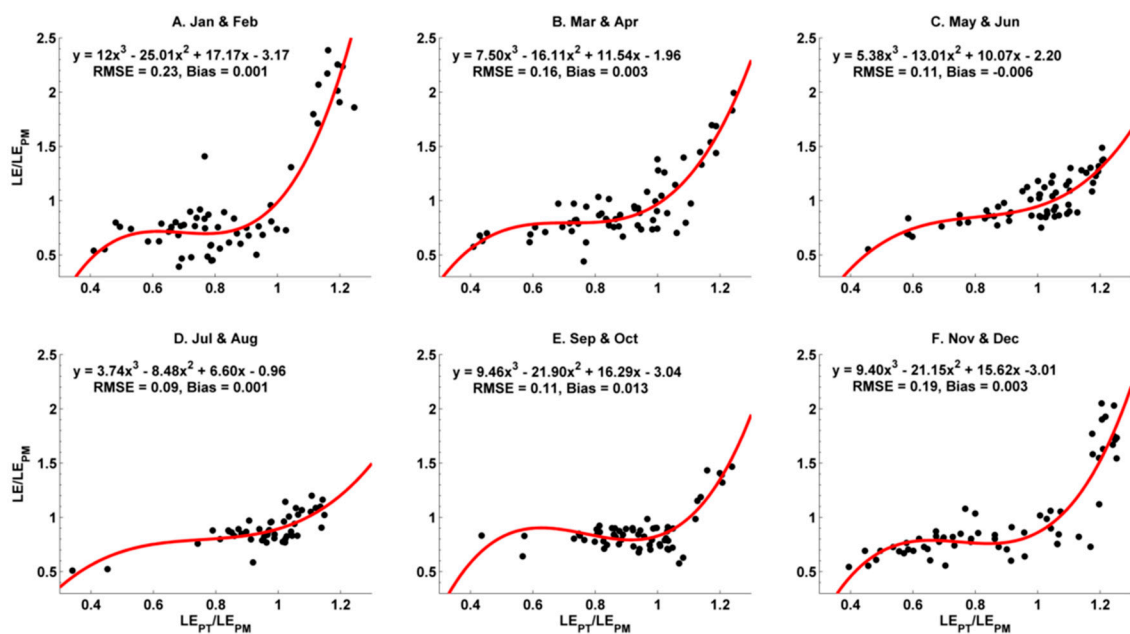
Figure 11. Quadratic fitting of x-y relationships under various water level conditions, where $x = LE_{PT}/LE_{PM}$, and $y = LE/LE_{PM}$. (**A**), Jan and Feb; (**B**), Mar and Apr; (**C**), May and Jun; (**D**), Jul and Aug; (**E**), Sep and Oct; (**F**), Nov and Dec. Red line represents fitted line and black circle represents the original data.

The magnitude order of LE_{PT} and LE_{PM} can be determined before the actual LE is estimated. Therefore, we further evaluated the performances of the AA and the NAA models under the $LE_{PT} \leq LE_{PM}$ and the $LE_{PT} > LE_{PM}$ conditions. When $LE_{PT} \leq LE_{PM}$, both the AA and the NAA models performed better during the high-water periods. However, the NAA model outperformed the AA model, with much smaller RMSE and absolute biases during all periods (Figure 12). The biases of the NAA model were even close to 0 during some of the periods. In contrast, the NAA model was comparable or slightly worse than the AA model under the $LE_{PT} > LE_{PM}$ condition.
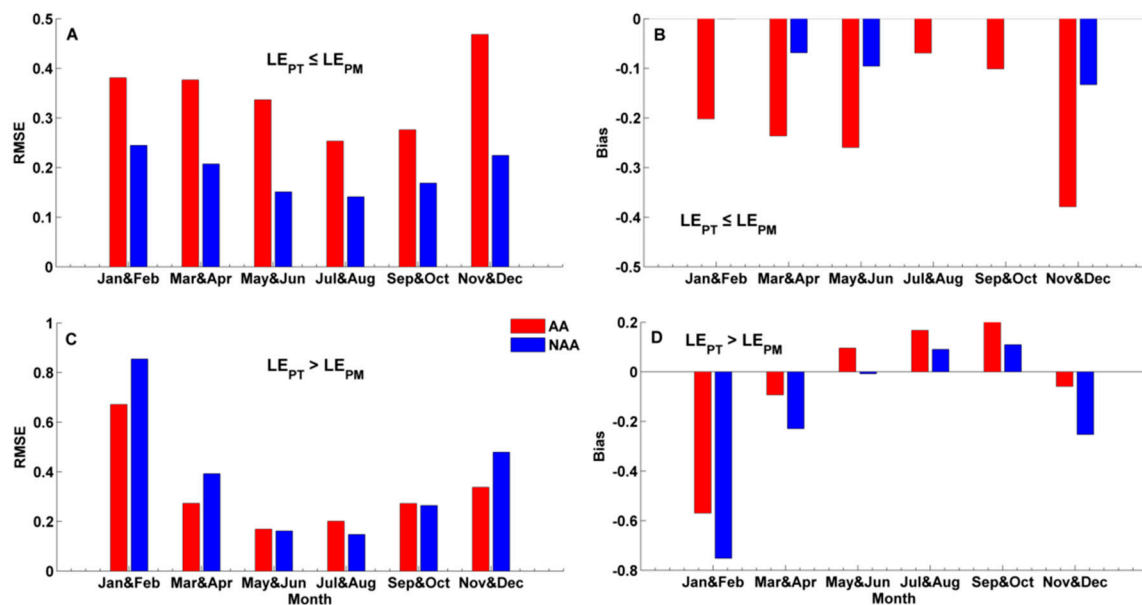
Figure 12. Performances of the AA and the NAA models under the $LE_{PT} \leq LE_{PM}$ (**A**) and (**B**) and the $LE_{PT} > LE_{PM}$ (**C**) and (**D**) conditions.

6. Conclusions

The CR models have been widely used due to their simple formulation and relatively few input requirements. However, although CR depicts the ET process as the land surface changes from completely wet to completely dry, few studies have compared the utility of CR models in different surface/atmosphere humidity conditions. In this study, we conducted a comparative study between the AA and the NAA models over a periodically inundated area of the Poyang Lake.

The results show that both the AA and the NAA models generally performed better under higher water level conditions. In addition, CR and the applicability of the CR models varied across different data categories. The value of B was typically 1.1 ± 1.4 when $LE \leq LE_{PT} \leq LE_{PM}$, and the AA model performed reasonably well in these cases. However, the value of B was generally negative in category 2 and the AA model had large negative biases in these cases. Under near-saturated air conditions, both the AA and the NAA models had negative biases.

Although different linear equations can separately fit the data points (x, y) in different categories, we were not able to classify the data points into different categories before ET was known. Compared to the AA model, the NAA model showed a more robust performance when $LE < LE_{PM}$. In humid climate areas, actual ET can be negatively or positively related to the evaporative demand of the air; our study shows that a higher-order CR model may provide more robust predictions in such conditions. New theoretical considerations of the boundary conditions by which the x-y relationship is established may be needed in future studies. Moreover, more data from humid climate regions are needed to study variations in the $LE_{PT}/LE_{PM} \sim LE/LE_{PM}$ relationships.

Author Contributions: Conceptualization, G.G. and Y.L.; methodology, G.G.; software, G.G.; validation, G.G., X.P. and X.Z.; formal analysis, G.G.; investigation, X.Z., M.L., and S.W.; resources, Y.L., M.L., and S.W.; data curation, X.Z., M.L., and S.W.; writing—original draft preparation, G.G.; writing—review and editing, G.G. and Y.L.; visualization, G.G. ; supervision, Y.L.; project administration, Y.L.; funding acquisition, G.G. and Y.L.

References

1. Tegos, A.; Malamos, N.; Efstratiadis, A.; Tsoukalas, I.; Karanasios, A.; Koutsoyiannis, D. Parametric modelling of potential evapotranspiration: A global survey. *Water* **2017**, *9*, 795. [CrossRef]

2. Law, B.E.; Falge, E.; Gu, L.; Baldocchi, D.D.; Bakwin, P.; Berbigier, P.; Davis, K.; Dolman, A.J.; Falk, M.; Fuentes, J.D.; et al. Environmental controls over carbon dioxide and water vapor exchange of terrestrial vegetation. *Agric. For. Meteorol.* **2002**, *113*, 97–120. [CrossRef]

3. Scott, R.L.; Huxman, T.E.; Cable, W.L.; Emmerich, W.E. Partitioning of evapotranspiration and its relation to carbon dioxide exchange in a chihuahuan desert shrubland. *Hydrol. Process.* **2006**, *20*, 3227–3243. [CrossRef]

4. Trenberth, K.E.; Smith, L.; Qian, T.T.; Dai, A.; Fasullo, J. Estimates of the global water budget and its annual cycle using observational and model data. *J. Hydrometeorol.* **2007**, *8*, 758–769. [CrossRef]

5. Li, Z.L.; Tang, R.L.; Wan, Z.M.; Bi, Y.Y.; Zhou, C.H.; Tang, B.H.; Yan, G.J.; Zhang, X.Y. A review of current methodologies for regional evapotranspiration estimation from remotely sensed data. *Sensors* **2009**, *9*, 3801–3853. [CrossRef] [PubMed]

6. Kalma, J.D.; McVicar, T.R.; McCabe, M.F. Estimating land surface evaporation: A review of methods using remotely sensed surface temperature data. *Surv. Geophys.* **2008**, *29*, 421–469. [CrossRef]

7. Wang, K.C.; Dickinson, R.E. A review of global terrestrial evapotranspiration: Observation, modeling, climatology, and climatic variability. *Rev. Geophys.* **2012**, *50*, 50. [CrossRef]

8. Jaksa, W.T.; Sridhar, V.; Huntington, J.L.; Khanal, M. Evaluation of the complementary relationship using noah land surface model and north american regional reanalysis (narr) data to estimate evapotranspiration in semiarid ecosystems. *J. Hydrometeorol.* **2013**, *14*, 345–359. [CrossRef]

9. Ramirez, J.A.; Hobbins, M.T.; Brown, T.C. Observational evidence of the complementary relationship in regional evaporation lends strong support for bouchet's hypothesis. *Geophys. Res. Lett* **2005**, *32*. [CrossRef]

10. Fisher, J.B.; Tu, K.P.; Baldocchi, D.D. Global estimates of the land-atmosphere water flux based on monthly avhrr and islscp-ii data, validated at 16 fluxnet sites. *Remote Sens. Environ.* **2008**, *112*, 901–919. [CrossRef]

11. Gao, Y.C.; Gan, G.J.; Liu, M.F.; Wang, J.F. Evaluating soil evaporation parameterizations at near-instantaneous scales using surface dryness indices. *J. Hydrol.* **2016**, *541*, 1199–1211. [CrossRef]

12. Gan, G.; Kang, T.; Yang, S.; Bu, J.; Feng, Z.; Gao, Y. An optimized two source energy balance model based on complementary concept and canopy conductance. *Remote Sens. Environ.* **2019**, *223*, 243–256. [CrossRef]

13. Brutsaert, W. Indications of increasing land surface evaporation during the second half of the 20th century. *Geophys. Res. Lett.* **2006**, *33*. [CrossRef]

14. Brutsaert, W.; Parlange, M.B. Hydrologic cycle explains the evaporation paradox. *Nature* **1998**, *396*, 30. [CrossRef]

15. Bouchet, R. Evapotranspiration reelle et potentielle, significantion climatique. *IAHS Publ.* **1963**, *62*, 134–142.

16. Brutsaert, W.; Stricker, H. Advection-aridity approach to estimate actual regional evapotranspiration. *Water Resour. Res.* **1979**, *15*, 443–450. [CrossRef]

17. Morton, F.I. Operational estimates of areal evapo-transpiration and their significance to the science and practice of hydrology. *J. Hydrol.* **1983**, *66*, 1–76. [CrossRef]

18. Granger, R.J. A complementary relationship approach for evaporation from nonsaturated surfaces. *J. Hydrol.* **1989**, *111*, 31–38. [CrossRef]

19. Granger, R.J. An examination of the concept of potential evaporation. *J. Hydrol.* **1989**, *111*, 9–19. [CrossRef]

20. Han, S.J.; Hu, H.P.; Yang, D.W.; Tian, F.Q. A complementary relationship evaporation model referring to the granger model and the advection-aridity model. *Hydrol. Process.* **2011**, *25*, 2094–2101. [CrossRef]

21. Brutsaert, W. A generalized complementary principle with physical constraints for land-surface evaporation. *Water Resour. Res.* **2015**, *51*, 8087–8093. [CrossRef]

22. Aminzadeh, M.; Roderick, M.L.; Or, D. A generalized complementary relationship between actual and potential evaporation defined by a reference surface temperature. *Water Resour. Res.* **2016**, *52*, 385–406. [CrossRef]

23. Szilagyi, J.; Jozsa, J. New findings about the complementary relationship-based evaporation estimation methods. *J. Hydrol.* **2008**, *354*, 171–186. [CrossRef]

24. Liu, S.M.; Sun, R.; Sun, Z.P.; Li, X.O.; Liu, C.M. Evaluation of three complementary relationship approaches for evapotranspiration over the yellow river basin. *Hydrol. Process.* **2006**, *20*, 2347–2361. [CrossRef]

25. Yu, J.; Zhang, Y.; Liu, C. Validity of the bouchet's complementary relationship at 102 observatories across china. *Sci. China Ser. D* **2009**, *52*, 708–713. [CrossRef]

26. Kahler, D.M.; Brutsaert, W. Complementary relationship between daily evaporation in the environment and pan evaporation. *Water Resour. Res.* **2006**, *42*. [CrossRef]

27. Crago, R.; Crowley, R. Complementary relationships for near-instantaneous evaporation. *J. Hydrol.* **2005**, *300*, 199–211. [CrossRef]

28. Szilagyi, J. On bouchet's complementary hypothesis. *J. Hydrol.* **2001**, *246*, 155–158. [CrossRef]

29. Szilagyi, J. On the inherent asymmetric nature of the complementary relationship of evaporation. *Geophys. Res. Lett.* **2007**, *34*. [CrossRef]

30. Brutsaert, W.; Li, W.; Takahashi, A.; Hiyama, T.; Zhang, L.; Liu, W.Z. Nonlinear advection-aridity method for landscape evaporation and its application during the growing season in the southern loess plateau of the yellow river basin. *Water Resour. Res.* **2017**, *53*, 270–282. [CrossRef]

31. Zhang, L.; Cheng, L.; Brutsaert, W. Estimation of land surface evaporation using a generalized nonlinear complementary relationship. *J. Geophys. Res. Atmos.* **2017**, *122*, 1475–1487. [CrossRef]

32. Liu, X.M.; Liu, C.M.; Brutsaert, W. Regional evaporation estimates in the eastern monsoon region of china: Assessment of a nonlinear formulation of the complementary principle. *Water Resour. Res.* **2016**, *52*, 9511–9521. [CrossRef]

33. Szilagyi, J.; Crago, R.; Qualls, R.J. Testing the generalized complementary relationship of evaporation with continental-scale long-term water-balance data. *J. Hydrol.* **2016**, *540*, 914–922. [CrossRef]

34. Priestley, C.H.B.; Taylor, R.J. Assessment of surface heat-flux and evaporation using large-scale parameters. *Mon. Weather Rev.* **1972**, *100*, 81–92. [CrossRef]

35. Penman, H.L. Natural evaporation from open water, bare soil and grass. *Proc. R. Soc. Lon. Ser. A* **1948**, *193*, 120–145.

36. Shuttleworth, W.J. Evaporation. In *Hand Book of Hydrology*; Maidment, D.R., Ed.; McGraw-Hill: New York, NY, USA, 1993.

37. Brutsaert, W. *Hydrology: An Introduction*; Cambridge University Press: New York, NY, USA, 2005.

38. Ye, X.C.; Zhang, Q.; Liu, J.; Li, X.H.; Xu, C.Y. Distinguishing the relative impacts of climate change and human activities on variation of streamflow in the poyang lake catchment, china. *J. Hydrol.* **2013**, *494*, 83–95. [CrossRef]

39. Wu, G.P.; Liu, Y.B. Capturing variations in inundation with satellite remote sensing in a morphologically complex, large lake. *J. Hydrol.* **2015**, *523*, 14–23. [CrossRef]

40. Wu, G.P.; Liu, Y.B. Combining multispectral imagery with in situ topographic data reveals complex water level variation in china's largest freshwater lake. *Remote Sens.* **2015**, *7*, 13466–13484. [CrossRef]

41. Liu, Y.B.; Wu, G.P.; Zhao, X.S. Recent declines in china's largest freshwater lake: Trend or regime shift? *Environ. Res. Lett.* **2013**, *8*, 014010. [CrossRef]

42. Liu, Y.; Wu, G. Hydroclimatological influences on recently increased droughts in china's largest freshwater lake. *Hydrol. Earth Syst. Sci.* **2016**, *20*, 93–107. [CrossRef]

43. Zhao, X.S.; Liu, Y.B. Phase transition of surface energy exchange in china's largest freshwater lake. *Agric. For. Meteorol.* **2017**, *244*, 98–110. [CrossRef]

44. Xu, C.Y.; Singh, V.P. Evaluation of three complementary relationship evapotranspiration models by water balance approach to estimate actual regional evapotranspiration in different climatic regions. *J. Hydrol.* **2005**, *308*, 105–121. [CrossRef]

45. Hobbins, M.T.; Ramirez, J.A.; Brown, T.C. The complementary relationship in estimation of regional evapotranspiration: An enhanced advection-aridity model. *Water Resour. Res.* **2001**, *37*, 1389–1403. [CrossRef]

46. Pettijohn, J.C.; Salvucci, G.D. Impact of an unstressed canopy conductance on the bouchet-morton complementary relationship. *Water Resour. Res.* **2006**, *42*. [CrossRef]

47. Yang, H.B.; Yang, D.W.; Lei, Z.D. Seasonal variability of the complementary relationship in the asian monsoon region. *Hydrol. Process.* **2013**, *27*, 2736–2741. [CrossRef]

48. Guo, X.F.; Liu, H.P.; Yang, K. On the application of the priestley-taylor relation on sub-daily time scales. *Bound. Lay Meteorol.* **2015**, *156*, 489–499. [CrossRef]

49. Assouline, S.; Li, D.; Tyler, S.; Tanny, J.; Cohen, S.; Bou-Zeid, E.; Parlange, M.; Katul, G.G. On the variability of the priestley-taylor coefficient over water bodies. *Water Resour. Res.* **2016**, *52*, 150–163. [CrossRef]

50. Han, S.J.; Tian, F.Q.; Hu, H.P. Positive or negative correlation between actual and potential evaporation? Evaluating using a nonlinear complementary relationship model. *Water Resour. Res.* **2014**, *50*, 1322–1336. [CrossRef]